# Enhanced optical Kerr nonlinearity of $MoS_2$ on silicon waveguides

**Linghai Liu,[1] Ke Xu,[2,3] Xi Wan,[1] Jianbin Xu,[1] Chi Yan Wong,[1,*] and Hon Ki Tsang[1]**

[1]*Department of Electronic Engineering, The Chinese University of Hong Kong, Shatin, Hong Kong, China*
[2]*Department of Electronic and Information Engineering, Shenzhen Graduate School, Harbin Institute of Technology, Shenzhen, China*
[3]*e-mail: kxu@hitsz.edu.cn*
**Corresponding author: cywong@ee.cuhk.edu.hk*

Received May 29, 2015; revised June 29, 2015; accepted July 11, 2015;
posted July 16, 2015 (Doc. ID 242019); published August 7, 2015

A quasi-two-dimensional layer of $MoS_2$ was placed on top of a silicon optical waveguide to form a $MoS_2$–silicon hybrid structure. Chirped pulse self-phase modulation measurements were carried out to determine the optical Kerr nonlinearity of the structure. The observed increase in the spectral broadening of the optical pulses in the $MoS_2$–silicon waveguide compared with the silicon waveguides indicated that the third-order nonlinear effect in $MoS_2$ is about 2 orders of magnitude larger than that in silicon. The measurements show that $MoS_2$ has an effective optical Kerr coefficient of about $1.1 \times 10^{-16}$ $m^2/W$. This work reveals the potential application of $MoS_2$ to enhance the nonlinearity of hybrid silicon optical devices. 

*OCIS codes:* (190.0190) Nonlinear optics; (190.3270) Kerr effect; (190.4400) Nonlinear optics, materials; (160.4330) Nonlinear optical materials.
http://dx.doi.org/10.1364/PRJ.3.000206

## 1. INTRODUCTION

Molybdenum disulfide ($MoS_2$) is a kind of transition metal dichalcogenide and has attracted increasing research interest in recent years because of its unique electronic and optical properties [1] that may lead to potential applications in high-performance electronic and optoelectronic devices. Single-layer $MoS_2$ consists of a molybdenum atomic plane sandwiched between two sulphur atomic layers. While bulk $MoS_2$ is an indirect bandgap (about 1.29 eV) semiconductor material, single-layer $MoS_2$ has a direct bandgap of about 1.90 eV [2]. Electrical mobility of 700 $cm^2/(V \cdot s)$ of multilayer exfoliated $MoS_2$ at room temperature has been reported [3], and an extremely high on–off ratio ($\sim 10^8$) field effect transistor was demonstrated with single-layer $MoS_2$ [3,4], which might not be achievable by graphene because of its zero bandgap [5]. Monolayer $MoS_2$ also showed good performance in ultrasensitive photodetectors (PDs) as active materials for optical detection in the ultraviolet to visible range [6]. Moreover, $MoS_2$ was found to be also suitable as a broadband saturable absorber operating at wavelengths in the visible to near-infrared spectral range [7,8]. $MoS_2$ has been used as a saturable absorber in femtosecond mode-locked lasers [7]. Due to the lack of inversion symmetry, odd-layered $MoS_2$ can have second-order nonlinear effects [9], which may be exploited for applications in optoelectronic devices.

Third-order nonlinear effects in $MoS_2$ were previously experimentally studied via the measurement of third-harmonic generation in the wavelength range from 1758 to 1980 nm [10]. The third-order nonlinear susceptibility obtained in that paper was $\chi^{(3)} \sim 10^{-19}$ $m^2/V$ at 1758 nm. To our knowledge, however, there has been no previous experimental investigation of the optical nonlinearity of $MoS_2$ at the wavelengths commonly used in telecommunications and silicon photonics. In this paper, a layer of $MoS_2$ prepared by chemical vapor deposition (CVD) was placed on the top of a silicon waveguide integrated with waveguide grating couplers. The interaction of the evanescent optical field in the waveguide with the layer of $MoS_2$ over the length of the waveguide produces changes in the spectra of optical pulses because of self-phase modulation (SPM). The refractive index of $MoS_2$ was obtained experimentally from the redshift of the center wavelength of the grating couplers after placing the $MoS_2$ on the grating coupler. A significant increase in broadening of pulses from the $MoS_2$–silicon waveguide compared to that from the bare silicon waveguide indicates enhancement of the optical Kerr nonlinear effect by the $MoS_2$ layer. Measurement of the spectral broadening also gave estimation of the optical Kerr nonlinear coefficient of $MoS_2$ at a wavelength of 1554.5 nm.

## 2. DEVICE FABRICATION

The silicon waveguide and grating were fabricated on a silicon-on-insulator wafer with a 340 nm silicon top layer and 2 μm buried oxide. Electron beam lithography (EBL) was used to define the waveguide and grating patterns after a layer of photoresist was formed by spin coating. The chip was developed and rinsed after EBL exposure, followed by etching with deep reactive-ion etching. The $MoS_2$ layer was prepared and transferred onto the silicon chip with methods similar to the techniques described in previous works [11–14]. Solid $MoO_3$ and S powders were used as precursors. Typically, ~50 mg $MoO_3$ (99.5% Sigma Aldrich) was placed in quartz boats and 0.5 g sulphur (99.5% Sigma Aldrich) was located upstream. The CVD growth was performed at atmospheric pressure with 500 sccm (sccm denotes cubic centimeters per minute at standard temperature and pressure) Ar as the protection gas. The growth temperature was around

 

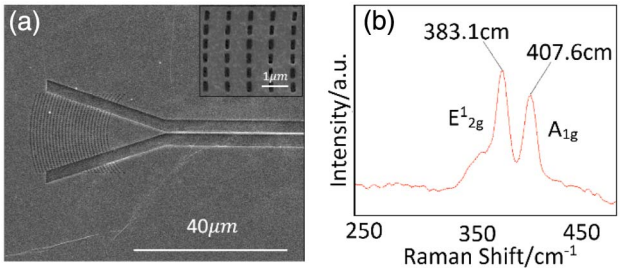


Fig. 1. (a) Scanning electron microscope image of one part of the device, with $MoS_2$ covering both the grating couplers and waveguide regions. As the whole area is covered by the material, significant contrast does not exist. Inset: magnified picture of the grating. (b) Measured Raman spectrum of the $MoS_2$ layer on the top of the waveguide region.

700°C–800°C. Figure 1(a) shows one set of grating and waveguide, with $MoS_2$ covering the top of both the grating coupler and waveguide regions. The inset shows the magnified picture for the grating coupler region. Figure 1(b) is the measured Raman spectrum of the $MoS_2$, which clearly shows that the $E^1_{2g}$ peak is located at about 383.1 $cm^{-1}$ and the $A_{1g}$ peak at about 407.6 $cm^{-1}$. A distance of 24.5 $cm^{-1}$ difference between the two peaks implies the multilayer nature of the $MoS_2$ layer, and the thickness was estimated to be ~10 nm with the above characteristics [15]. The thickness was also confirmed by the measurement performed by a tapping mode atomic force microscope (Dimension Icon System from Bruker).

## 3. REFRACTIVE INDEX OF $MoS_2$

Transmission spectra of the devices were measured using a tunable laser at low power before and after transferring $MoS_2$ on to the devices, which are shown in Fig. 2(a). There was about 15.0 nm redshift of the center wavelength induced by the $MoS_2$ layer, which results from the increased effective grating period because of the larger refractive index of the 10 nm thick $MoS_2$.

Finite-difference time-domain (FDTD) simulation for gratings was carried out to estimate the refractive index of the $MoS_2$ layer, which is shown in Fig. 2(b). The simulation parameters needed to produce a similar shift as the experimental results suggest that the refractive index $n$ was about 4.5, which is also consistent with the previous report [16]. The loss induced by top-layer $MoS_2$ could be attributed to the reflection of light by $MoS_2$ because of the high refractive index. The effective coupling efficiency of one grating coupler, about

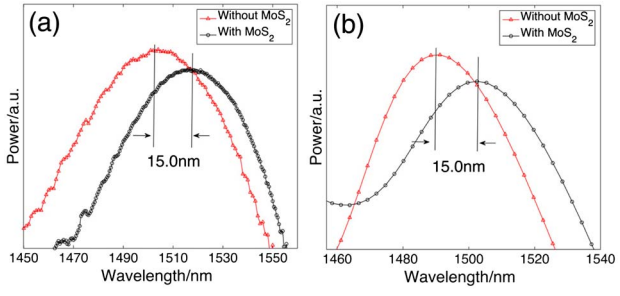


Fig. 2. (a) Experimental results of the transmission spectra of the gratings. Significant redshift of the center wavelengths was induced by the $MoS_2$ layer. (b) FDTD simulation result for the redshift of the grating to estimate the refractive index of $MoS_2$.

–6.7 dB, was recorded for determining the input power to the $MoS_2$–silicon waveguide used in following experiments where third order nonlinear coefficient of $MoS_2$ will be estimated.

## 4. SPM MEASUREMENTS AND KERR COEFFICIENT CALCULATION

After transferring $MoS_2$ onto the silicon waveguide, optical pulses in the waveguide will experience nonlinear SPM from third-order nonlinear effects in silicon and $MoS_2$, resulting in a broadening of the optical spectrum. Measuring the effective broadened spectrum output from the $MoS_2$–silicon waveguide and calculating optical mode distribution in the waveguide would allow the third-order nonlinear coefficient of $MoS_2$ to be obtained. The experimental setup is shown in Fig. 3. Optical pulses at a repetition rate of 1 MHz were produced by gain-switching a distributed feedback (DFB) grating diode laser. The pulses had a full width at half-maximum pulse width of about 56 ps and a center wavelength of 1554.5 nm. The pulses were coupled into the waveguide and the spectral broadening at the output was recorded. A small fraction of the input pulse was directed to the PD for monitoring the average power input to the device under test (DUT). The DUT could be a $MoS_2$–silicon waveguide, a bare silicon waveguide, or single-mode fiber.

The optical pulses from the gain-switched DFB laser were chirped and the spectrum contains many detailed features, which are difficult to model. Instead of calculating the nonlinear phase shift in the SPM directly, the same spectral broadening as obtained from the $MoS_2$–silicon waveguide was obtained by SPM in a known length of standard single-mode fiber. The broadened spectrum from the $MoS_2$–silicon waveguide was first measured, then the DUT was changed to be the single-mode fiber, to which the input power was tuned to make the output spectrum from the fiber match that obtained from the $MoS_2$–silicon waveguide. With the input power and known parameters of the single-mode fiber, the nonlinear phase shift in the fiber could be calculated, and it is equivalent to that experienced by the pulse in the $MoS_2$–silicon waveguide. To ensure that the shape of the input pulse spectra to the $MoS_2$–silicon waveguide and the single-mode fiber were the same, the configuration of the gain-switched laser, erbium-doped fiber amplifier (EDFA) and the bandpass filter (BPF) were unchanged throughout the experiments. The input power to the DUT was adjusted only by a mechanical optical attenuator (ATT). In addition, the fiber between the ATT and the DUT was made as short as possible to avoid spectrum change due to nonlinear effects in this section of fiber. This was verified by measuring the output spectra from the input port to the DUT under various attenuation values, and no significant change in the shape of spectra was found.

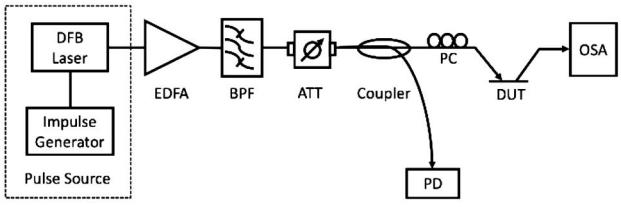


Fig. 3. Experimental setup used for measuring the third-order nonlinear coefficient of $MoS_2$. The gain-switched DFB diode laser was used as pulse source. PC, polarization controller.

The output spectra from the $MoS_2$–silicon waveguide and single-mode fiber were then measured and recorded with the optical spectrum analyzer (OSA). The results are shown in Fig. 4. In Fig. 4, the black curve shows the input spectrum, while the red curve and the blue curve correspond to broadened output spectra from the $MoS_2$–silicon waveguide and the bare silicon waveguide, respectively. Evidently, the pulse broadening effect is more significant in the $MoS_2$–silicon waveguide, which indicates a larger nonlinear Kerr coefficient of the $MoS_2$ layer. The calculation of the coefficient is carried out as follows.

Nonlinear phase shift experienced by the pulse in $MoS_2$–silicon waveguide is given by [17,18]

$$\phi_{nl}^{\mathrm{MOS}} = \frac{2\pi \Delta n_{\mathrm{eff}} L_{\mathrm{eff}}}{\lambda}, \tag{1}$$

where $\Delta n_{\mathrm{eff}}$ is effective nonlinear refractive index of the $MoS_2$–silicon waveguide, $\lambda$ is the vacuum center wavelength of the pulse, and $L_{\mathrm{eff}} = [1 - \exp(-\alpha L)]/\alpha$ is the effective length of the structure ($L$ corresponds to the physical length). Change in effective index due to the nonlinear optical Kerr effect could be treated as a small perturbation. According to the first-order perturbation theory [19], $\Delta n_{\mathrm{eff}}$ can be expressed as

$$\Delta n_{\mathrm{eff}} = \frac{\iint_{\infty} \Delta \epsilon_r |E|^2 \mathrm{d}x\mathrm{d}y}{2Z_o \iint_{\infty} \mathrm{Re}\{\boldsymbol{E}^* \times \boldsymbol{H}\} \cdot \hat{\boldsymbol{e}}_z \mathrm{d}x\mathrm{d}y}, \tag{2}$$

where $\Delta \epsilon_r$ is the change of dielectric constant, and $Z_0$ is the impedance of the vacuum. The pulse is assumed to propagate along the $z$ direction. The integral in Eq. (2) covers the whole cross section of the structure. Denoting the Kerr coefficient as $n_2$, the change of dielectric constant can then be approximated by

$$\begin{aligned} \epsilon_r &= (n + \Delta n)^2 \approx n^2 + 2n\Delta n, \\ \Delta \epsilon_r &\approx 2n\Delta n = n^2 n_2 c \epsilon_0 |E|^2, \end{aligned} \tag{3}$$

where $n$ is refractive index, $\Delta n = n_2 I$ is the small change of refractive index due to the Kerr effect, $I = \frac{1}{2} c \epsilon_0 n |E|^2$ is local optical intensity, $\epsilon_0$ is vacuum permittivity, and $c$ is the speed of light in vacuum space.

For the high index contrast waveguide, $\boldsymbol{H} \neq \frac{c\epsilon}{n_{\mathrm{eff}}} \hat{\boldsymbol{e}}_z \times \boldsymbol{E}$. Therefore, the denominator in Eq. (2), which is $\iint_{\infty} \mathrm{Re}\{\boldsymbol{E}^* \times \boldsymbol{H}\} \cdot \hat{\boldsymbol{e}}_z \mathrm{d}x\mathrm{d}y$ cannot be simplified as the conventional method [20]. Fortunately, from the relationship of power flux and energy density flow [20], we have

$$\frac{1}{2} \iint_{\infty} \mathrm{Re}\{\boldsymbol{E}^* \times \boldsymbol{H}\} \cdot \hat{\boldsymbol{e}}_z \mathrm{d}x\mathrm{d}y = \frac{1}{2} v_g \iint_{\infty} \epsilon |E|^2 \mathrm{d}x\mathrm{d}y, \tag{4}$$

where $v_g$ is group velocity for the pulse in the waveguide and $\epsilon = \epsilon_0 n^2$. With Eqs. (1)–(4), one can finally get that

$$\Delta n_{\mathrm{eff}} = n_g^2 \cdot \frac{P_o}{A_{\mathrm{eff}}} \cdot \frac{\sum_A n_{2A} \iint_A \epsilon |E|^4 \mathrm{d}x\mathrm{d}y}{\iint_{\infty} \epsilon |E|^4 dxdy}, \tag{5}$$

where $n_g$ is group index; $A$ denotes the $MoS_2$, silicon, and silicon dioxide regions, and $A_{\mathrm{eff}}$ is defined as

$$A_{\mathrm{eff}} = \frac{[\iint_{\infty} \epsilon |E|^2 \mathrm{d}x\mathrm{d}y]^2}{\epsilon_o \iint_{\infty} \epsilon |E|^4 \mathrm{d}x\mathrm{d}y}. \tag{6}$$

Integration of the amplitude of the electric field can be obtained by mode distribution over the $MoS_2$–silicon structure from the simulation, which is shown in Fig. 5.

Nonlinear phase shift of the single-mode fiber can be calculated with the following equation [18]:

$$\phi_{nl}^{\mathrm{Fiber}} = \frac{2\pi n_{2f} P_{0f} L_{\mathrm{eff}}}{\lambda A_{\mathrm{eff}}^f}, \tag{7}$$

where $n_{2f}$ is the Kerr coefficient of the fiber, $P_0$ the peak power input to the fiber, and $A_{\mathrm{eff}}^f$ the mode effective area, which could also be calculated with the mode distribution from simulation for the fiber. In this paper, a piece of 102 m standard single-mode fiber was used, whose linear loss $\alpha$ is ~0.4 dB/km, and $n_{2f} \sim 2.25 \times 10^{-20}$ $\mathrm{m}^2/\mathrm{W}$ [18]. $P_0$ was adjusted by ATT in Fig. 3, so as to make the output spectrum from the fiber match that of the $MoS_2$–silicon waveguide, so that

$$\phi_{nl}^{\mathrm{MOS}} = \phi_{nl}^{\mathrm{Fiber}}. \tag{8}$$

With this method and Eqs. (1)–(8), the Kerr coefficient of $MoS_2$ was extracted to be about $1.1 \times 10^{-16}$ $\mathrm{m}^2/\mathrm{W}$, with a measurement uncertainty around 40%. The uncertainty comes from several aspects. First, the coupling efficiency per grating was estimated from the total insertion loss (IL) of the waveguide at low input power. The efficiency is modeled to follow normal distribution whose mean is half of the IL, and the $3\sigma$ region covers half of the IL. So the actual input power to the

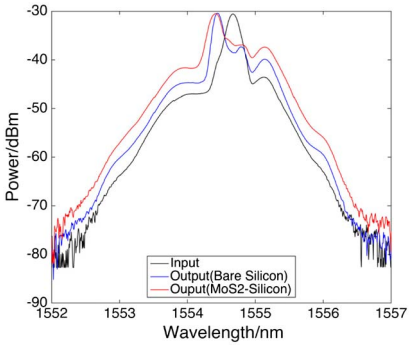


Fig. 4. Input and output spectrum of $MoS_2$–silicon waveguide and bare silicon waveguide. Black curve is the input spectrum, while the red and blue curves are from the output of the $MoS_2$–silicon waveguide and the bare silicon waveguide, respectively.

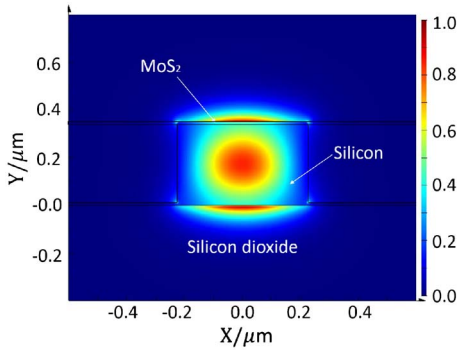


Fig. 5. Optical intensity distribution of the $MoS_2$–silicon waveguide structure, which was used for nonlinear refractive index calculation. $MoS_2$ layer, silicon core, and silicon dioxide substrate are indicated.

$MoS_2$–silicon waveguide accounts for a large uncertainty factor. Second, the Kerr coefficient of silicon $n_{2si}$ was used in calculating the coefficient for $MoS_2$ [Eq. (4)], and it also has a range of uncertainty based on previous measured results [21]. $n_{2si} = 4.5 \times 10^{-18}$ $m^2/W$ is applied here. Third, the equivalent nonlinear phase shift determined from the fiber also has uncertainty in matched input power to the fiber, accounting for the uncertainty in determining the nonlinear phase shift. These three factors together are responsible for the overall uncertainty of around 40%. Nevertheless, the deduced coefficient can provide a reference for the order of magnitude. It is 2 orders larger than that of silicon, and from the equation [22]

$$n_2 = \frac{3}{4\epsilon_0 c n^2}\chi^{(3)}, \tag{9}$$

where $n$ is the refractive of $MoS_2$, which is about 4.5 from the result above, the third-order susceptibility $\chi^{(3)}$ of $MoS_2$ is thus about $7.9 \times 10^{-18}$ $m^2/V$. The result is 1 order of magnitude larger than the value measured at 1758 nm in work by Wang *et al.* [10].

## 5. CONCLUSIONS

In conclusion, a quasi-two-dimensional sheet of $MoS_2$ was transferred on top of a silicon waveguide and the optical parameters were measured at telecommunication wavelength. The refractive index was extracted to be ~4.5 from the redshift of the grating couplers. The third-order nonlinear coefficient and susceptibility of $MoS_2$ was determined from SPM in the $MoS_2$–silicon structure. The nonlinear refractive index of the material was extracted to be about $1.1 \times 10^{-16}$ $m^2/W$, and the corresponding susceptibility is about $7.9 \times 10^{-18}$ $m^2/V$. The high nonlinear coefficient of $MoS_2$ at telecommunication wavelengths offers opportunities to use it to enhance the optical nonlinearity of hybrid silicon photonic waveguides for nonlinear optical devices.

## ACKNOWLEDGMENT

This work was fully funded by Hong Kong Research Grants Council research project nos. GRF416913, N_CUHK405/12, AoE/P-02/12, CUHK1/CRF/12G. The authors would like to thank Qijie Xie for the technical support.

## REFERENCES

1. Q. H. Wang, K. Kalantar-Zadeh, A. Kis, J. N. Coleman, and M. S. Strano, "Electronics and optoelectronics of two-dimensional transition metal dichalcogenides," Nat. Nanotechnol. **7**, 699–712 (2012).
2. K. F. Mak, C. Lee, J. Hone, J. Shan, and T. F. Heinz, "Atomically thin $MoS_2$: a new direct-gap semiconductor," Phys. Rev. Lett. **105**, 136805 (2010).
3. S. Das, H.-Y. Chen, A. V. Penumatcha, and J. Appenzeller, "High performance multilayer $MoS_2$ transistors with scandium contacts," Nano Lett. **13**, 100–105 (2012).
4. B. Radisavljevic, A. Radenovic, J. Brivio, V. Giacometti, and A. Kis, "Single-layer $MoS_2$ transistors," Nat. Nanotechnol. **6**, 147–150 (2011).
5. K. Novoselov, A. K. Geim, S. Morozov, D. Jiang, M. Katsnelson, I. Grigorieva, S. Dubonos, and A. Firsov, "Two-dimensional gas of massless Dirac fermions in graphene," Nature **438**, 197–200 (2005).
6. O. Lopez-Sanchez, D. Lembke, M. Kayci, A. Radenovic, and A. Kis, "Ultrasensitive photodetectors based on monolayer $MoS_2$," Nat. Nanotechnol. **8**, 497–501 (2013).
7. H. Liu, A.-P. Luo, F.-Z. Wang, R. Tang, M. Liu, Z.-C. Luo, W.-C. Xu, C.-J. Zhao, and H. Zhang, "Femtosecond pulse erbium-doped fiber laser by a few-layer $MoS_2$ saturable absorber," Opt. Lett. **39**, 4591–4594 (2014).
8. F. Wang, S. Xu, Y. Feng, Y. Li, X. Zhang, Y. Xu, and J. Wang, "Characteristics of saturable absorption of $MoS_2$ films in the visible to near-infrared range," in *Asia Communications and Photonics Conference* (Optical Society of America, 2014), paper ATh4B.5.
9. X. Yin, Z. Ye, D. A. Chenet, Y. Ye, K. O'Brien, J. C. Hone, and X. Zhang, "Edge nonlinear optics on a $MoS_2$ atomic monolayer," Science **344**, 488–490 (2014).
10. R. Wang, H.-C. Chien, J. Kumar, N. Kumar, H.-Y. Chiu, and H. Zhao, "Third-harmonic generation in ultrathin films of $MoS_2$," ACS Appl. Mater. Interfaces **6**, 314–318 (2013).
11. Y.-H. Lee, L. Yu, H. Wang, W. Fang, X. Ling, Y. Shi, C.-T. Lin, J.-K. Huang, M.-T. Chang, and C.-S. Chang, "Synthesis and transfer of single-layer transition metal disulfides on diverse surfaces," Nano Lett. **13**, 1852–1857 (2013).
12. Y.-H. Lee, X.-Q. Zhang, W. Zhang, M.-T. Chang, C.-T. Lin, K.-D. Chang, Y.-C. Yu, J. T.-W. Wang, C.-S. Chang, L.-J. Li, and T.-W. Lin, "Synthesis of large-area $MoS_2$ atomic layers with chemical vapor deposition," Adv. Mater. **24**, 2320–2325 (2012).
13. S. Najmaei, Z. Liu, W. Zhou, X. Zou, G. Shi, S. Lei, B. I. Yakobson, J.-C. Idrobo, P. M. Ajayan, and J. Lou, "Vapour phase growth and grain boundary structure of molybdenum disulphide atomic layers," Nat. Mater. **12**, 754–759 (2013).
14. A. M. van der Zande, P. Y. Huang, D. A. Chenet, T. C. Berkelbach, Y. You, G.-H. Lee, T. F. Heinz, D. R. Reichman, D. A. Muller, and J. C. Hone, "Grains and grain boundaries in highly crystalline monolayer molybdenum disulphide," Nat. Mater. **12**, 554–561 (2013).
15. C. Lee, H. Yan, L. E. Brus, T. F. Heinz, J. Hone, and S. Ryu, "Anomalous lattice vibrations of single-and few-layer $MoS_2$," ACS Nano **4**, 2695–2700 (2010).
16. C.-C. Shen, Y.-T. Hsu, L.-J. Li, and H.-L. Liu, "Charge dynamics and electronic structures of monolayer $MoS_2$ films grown by chemical vapor deposition," Appl. Phys. Express **6**, 125801 (2013).
17. R. H. Stolen and C. Lin, "Self-phase-modulation in silica optical fibers," Phys. Rev. A **17**, 1448–1453 (1978).
18. G. P. Agrawal, *Nonlinear Fiber Optics* (Academic, 2007).
19. T. Baehr-Jones, M. Hochberg, C. Walker, E. Chan, D. Koshinz, W. Krug, and A. Scherer, "Analysis of the tuning sensitivity of silicon-on-insulator optical ring resonators," J. Lightwave Technol. **23**, 4215–4221 (2005).
20. J. T. Robinson, K. Preston, O. Painter, and M. Lipson, "First-principle derivation of gain in high-index-contrast waveguides," Opt. Express **16**, 16659–16669 (2008).
21. H. Tsang and Y. Liu, "Nonlinear optical properties of silicon waveguides," Semicond. Sci. Technol. **23**, 064007 (2008).
22. T. Schneider, *Nonlinear Optics in Telecommunications* (Springer, 2004).